Article

Influence of Contact Interface Friction on Plastic Deformation of Stretch-Bend Forming

Shengfang Zhang, Guangming Lv [ID], Fujian Ma, Ziguang Wang and Yu Liu *[ID]

School of Mechanical Engineering, Dalian Jiaotong University, Dalian 116028, China; zsf@djtu.edu.cn (S.Z.); lv0527@163.com (G.L.); mafujianyx@163.com (F.M.); wangzg@djtu.edu.cn (Z.W.)
* Correspondence: liuyu_ly12@126.com

Abstract: The contact interface friction between the specimen and the mold during the stretch-bend is a complex interactive process. Friction causes the uneven distribution of tensile stress on the specimen, which affects the plastic flow of the forming material and the spring-back after forming. In this paper, the analytical model of frictional shear stress and tensile stress distribution in the contact mold segment of the stretch and bend synchronous loading stage was established. The influence law of friction coefficient and contact mold angle on the stress–strain distribution of the specimen contact mold segment was discussed. The effect of key factors affecting the friction state of the contact interface (mold surface roughness and contact mold angle) on the shrinkage deformation of the cross-section and the tensile deformation gradient of the specimen was analyzed by equivalent stretch-bend forming experiments. The results showed that the smaller the surface roughness of the mold was, the better the friction state of the contact interface was, the plastic deformation of the specimen was more uniform, and the difference between the section shrinkage and elongation of the contact mold segment and the suspension segment was smaller. Reducing the contact mold angle of the stretch-bend can bring down the tensile stress difference at both ends of the contact mold segment of the specimen so that the section shrinkage and tensile elongation of the contact mold segment and the suspension segment tend to be consistent.

Keywords: aluminum alloy profiles; stretch-bend forming; friction coefficient; plastic deformation; deformation gradient

1. Introduction

With the speed of high-speed railroad operations constantly refreshing, the development of the high-speed railway is entering the post high-speed railway era [1]. The structural strength of the high-speed train body has become one of the bottlenecks restricting the further development of high-speed railways [2]. The high-speed train body is mainly welded with high-strength, complex, cross-sectional aluminum alloy profiles stretch-bend-formed structural parts, which put forward higher requirements for the stretch-bend forming accuracy of aluminum alloy profiles structural parts [3].

Stretch-bend forming applies tangential tension to the ends of the profile during bending contact with the mold to reduce the stress difference between the inner and outer layers, which changes the internal stress distribution state of the cross-section and realizes the plastic forming processing for aluminum alloy profiles with large curvature and complex cross-sections [4]. In the process of stretch-bend forming, the friction of the contact interface between the stretch-bend mold and the profile is inevitable. With the increase of the contact mold angle, the contact interface changes continuously, and the frictional shear stress distribution is not uniform [5]. The tensile stress along the thickness and length of the specimen is distributed in a gradient, resulting in uneven plastic deformation of the stretch-bend specimen. Consequently, internal stress is also non-uniformly distributed after unloading, which makes it difficult to control spring-back and, therefore, dramatically

decreases the forming accuracy. The contact interface friction of stretch-bend forming is a cumulative and superimposed dynamic process, which is closely related to some factors, such as material properties, surface roughness, and friction conditions [6,7].

With the wide application of the profile stretch-bend forming process in the processing of large-scale curved structural parts, a lot of research work has been carried out on this process by researchers from different countries. Liang et al. [8] studied the influence of the bending angle of multi-point stretch-bend on the section deformation of the parts by using the ABAQUS finite element analysis method and predicted the forming quality control curve by the support vector regression method. Chen et al. [9] analyzed the spring-back of multi-point flexible stretch-bend forming of Y-section profiles under different process parameters. The effects of process parameters such as horizontal bending radius, vertical bending radius, transition length, rolling mold radius, and wall thickness of the profile on spring-back deviation were discussed. Liu et al. [10] investigated the spring-back characteristics of Z and T-sections aluminum lithium alloy stretch-bend forming using plastic deformation theory, explicit and implicit finite element theory, and experimental methods. The spring-back after unloading is caused by the high strength and modulus of elasticity of the aluminum-based alloy. In addition, the bending radius is closely related to the spring-back radius; the larger the bending radius, the larger the spring-back radius. Liu et al. [11] conducted a finite element simulation analysis of the stretch-bend process of aluminum alloy profiles, showing that increasing the complementary elongation reduces contour error and spring-back amount of the profile, but increases the section distortion and spatial distortion. A backtracking method was proposed to optimize the supplemental stretch rate. Liu et al. [12] studied the hot stretch-bending process of U-shaped titanium by applying numerical and experimental approaches. The electro–thermal–mechanical multi-fields coupling finite element model for U-shaped titanium extrusion hot stretch-bending was established by sequential numerical simulation between electro-thermal coupling and thermal-mechanical coupling. The optimal process parameters for hot stretch-bending of U-shaped extrusion were optimized and the spring-back after hot stretch-bend was evaluated. Welo and Ma [7,13] proposed a new flexible 3D stretch-bending process. Using experimental and numerical approaches, the capabilities of the forming method and machine were verified, and the characteristics and mechanisms were thoroughly explored. It was found that bending radius, friction, local deformation, and clamping have an obvious influence on forming quality. Maati et al. [14], through numerical simulations, demonstrated the influence of constitutive modeling on the prediction of the degree of spring-back in the case of a stretch-bending test. The spring-back depends closely on the material anisotropy. The final spring-back is greater in the direction of 0° for a low value of clamping force. Uemori et al. [15] proposed an explicitly theoretical analysis method based on the maximum load criterion that can easily and rapidly allow us to predict the fracture and spring-back of high-tensile-strength steel sheets by using two no-dimensional parameters (ultimate tensile ratio and ratio of plate thickness to bending radius). Gu et al. [16] conducted a finite element simulation analysis of the stretch-bend process of variable curvature L-section aluminum alloy profiles. The forming accuracy of complex curvature stretch-bend forming structural parts is improved by spring-back compensation for the mold surface curve.

The material properties, cross-sectional shape, and the amount of stretching all affect the amount of spring-back in the stretch-bend forming process. However, the increase of tensile stress will lead to uneven deformation of the specimen and increase the risk of specimen fracture since spring-back is caused by internal stress redistribution during unloading. The uneven plastic deformation will produce local stress concentration, which will increase the amount of spring-back and also intensify cross-sectional distortion. Han [17] obtained the effect law of contact pressure on the friction coefficient through draw-bending experiments of U-section specimens. When the contact pressure is small, the friction coefficient of the contact interface does not change much, and when the contact pressure is large, the friction coefficient of the contact interface increases with the increase of the contact pressure.

The change of the friction coefficient caused by the contact pressure affects the contact stress distribution of the specimen, which leads to the difference in the amount of spring-back. Fox et al. [18] conducted a test on the friction coefficient of sheet drawing and forming and established a mathematical model to describe the friction coefficient under different contact conditions. Liu et al. [19–21] found an analytical model for rotational tensile bending section deformation of thin-walled rectangular tubes and studied the effects of die constraint and interfacial friction on section deformation. The best combination of friction coefficient and minimum cross-sectional distortion was obtained by the rotary draw bending process tests. Guan et al. [22] analyzed the drawing and bending stress state of the sheet and established the relationship between friction coefficient and spring-back angle. The results showed that the frictional force is beneficial for reducing spring-back, but it is difficult to transfer the tensile force uniformly to all sections of the workpiece as the effect of friction force, which makes the specimen deformation uneven. Yang et al. [23], using explicit finite element simulation combined with physical experiments, explored the underlying effects of friction on bending behaviors from multiple aspects such as wrinkling, wall thickness variation, and cross-section deformation. Zhang et al. [24] studied the residual stress distribution of a 2026-T3511 aluminum alloy asymmetric T-section beam under displacement-controlled stretch-bend. A two-step numerical simulation was performed to predict the residual stress superposition in the quenching and subsequent mechanical processes. The spatial variation of the residual stresses in a stretch-bend beam can be mainly attributed to nonuniform plastic deformation through the thickness and longitudinal direction, which is caused by the combined load. Muranaka et al. [25] developed a new "rubber-assisted stretch bending method" by which elastic rubber can be partially applied to the surface of a die for the uniform bending with a constant curvature radius. The spring-back decreased by 21% in comparison with the crank motion simple bending by using ordinary metal dies. Xiang et al. [5] stated that tangential friction occurred at the rubber/metal interface during friction-assisted stretch-bend. Tangential friction assists in modifying stress distribution in the loading process. Liang et al. [26] studied the deformation difference between the contact zone and non-contact zone of profile and roller dies. The results showed that the pre-stretching amount has no obvious effect on the profile web heights in the contact and non-contact areas. However, the profile web thickness becomes thinner at each contact area away from the fixture, while the non-contact area thickness does not change significantly.

The stretch-bend forming process is described and discussed in the above research, including the influence of the contact interface friction between the stretch-bend specimen and the mold on the overall spring-back of the forming specimen after unloading. However, the influence of specific parameters of contact interface friction on the plastic flow of materials in the forming process was not concerned. Since the variation of the contact interface friction coefficient in stretch-bend forming is complex, it is necessary to explore the law of the key parameters affecting the friction state of the contact interface on the plastic flow of the formed specimen.

In this paper, the influence of the contact interface friction state (surface roughness of the mold and the angle of the contact mold) on the plastic deformation of a forming specimen was studied during the stretch-bend forming process. The stress state of the contact interface of the stretch-bend forming specimen was analyzed, and the analytical formula of the cross-section stress-strain distribution of the contact mold segment of the stretch-bend forming specimen was established. An equivalent stretch-bend forming experiment was designed based on the discrete step-by-step loading characteristics of the stretch-bend forming trajectory. By measuring the cross-section width and strain grid of the stretch-bend specimen, the influence law of the specimen plastic deformation with different die surface roughness and die-attaching angle was obtained, which indirectly verifies the stress–strain distribution of the specimen's cross-section. It provides a necessary reference for establishing variable increment (variable tensile increment and variable wrapping angle) trajectory optimization method.

2. Theoretical Analysis of Plastic Deformation in Stretch-Bend Forming

In the process of stretch-bend forming, the seemingly smooth surface of the stretch-bend specimen and the mold is an uneven rough surface. The high contact pressure of the contact interface between the profile and the mold is due to the tangential tension of the stretch-bend. According to Coulomb's law of friction, there will be friction between the contact interface of the profile and the mold, which hinders the plastic deformation of the profile. Since stretch-bend forming is the process of the specimen bending and sticking mold, the specimen is continuously bent toward the mold to fit the mold. During this time, the contact interface and contact pressure change complexly in real-time.

2.1. Force Analysis of Stretch-Bend Forming

The aluminum profile stretch-bend forming process can be divided into three stages: pre-stretch, stretch-bend, and complemental stretch. In the stage of stretch and bend synchronous loading, the specimen plastic deformation, and elongation under tensile load take place. The plastic sliding friction occurs due to the relative sliding between the specimen and the mold contact interface. With the increase of bend contact mold angle, the contact surface between the specimen and the mold keeps increasing continuously. The frictional shear stress on the surface of the specimen contact mold segment is opposite to the direction of tangential tension, which impedes the plastic flow of the specimen surface material and also changes the distribution of the shear stress along the thickness direction of the specimen, affecting the uniformity of plastic deformation.

The following basic assumptions are made for force analysis during stretch and bend synchronous loading.

(1) Section assumption: It is assumed that the sections before and after stretch-bend are flat, the section before stretch-bend is perpendicular to the axis of the profile, and the section after stretch-bend is perpendicular to the tangent of the neutral axis;

(2) Stress assumption: It is assumed that each element of the specimen is in a state of uniaxial tension or uniaxial compression during the stretch-bend forming process;

(3) Material elastic-plasticity assumption: It is assumed that the material is a homogeneous, continuous, and isotropic elastic–plastic deformation body. The elastic–plastic deformation conforms to the loading and unloading deformation law of classical elastic–plastic theory.

The force in the stretch-bend forming process is shown in Figure 1. In the figure, F is the axial tension force; R is the radius of the mold; ρ is the bending radius of the neutral layer of the profile; M is the total bending moment; F_f is the frictional force on the contact mold segment, and the direction is along the tangent direction of the mold arc; F_N is the positive pressure of the profile on the mold, and the direction is perpendicular to the contact surface.

Figure 1 shows the bending and tensile deformation under the combined action of bending moment and tensile force. The contact pressure between the specimen and the mold causes a frictional shear force on the contact surface opposite to the sliding direction of plastic deformation. Due to the continuity of the material, the frictional shear force produces a shearing effect on the plastic deformation section of the specimen. The Coulomb friction coefficient is used to characterize the shear friction force of the contact surface, as shown in Equation (1) [27]. The shear friction coefficient is used to characterize the shear action inside the workpiece, as shown in Equation (2) [28].

$$f = \frac{F_f}{F_N} \tag{1}$$

$$m = \frac{\tau_m}{\sigma_n} \tag{2}$$

where, the F_f is the friction of the contact surface; F_N is the positive pressure of the contact surface; τ_m is the frictional shear stress; σ_n is the shear strength of the material.
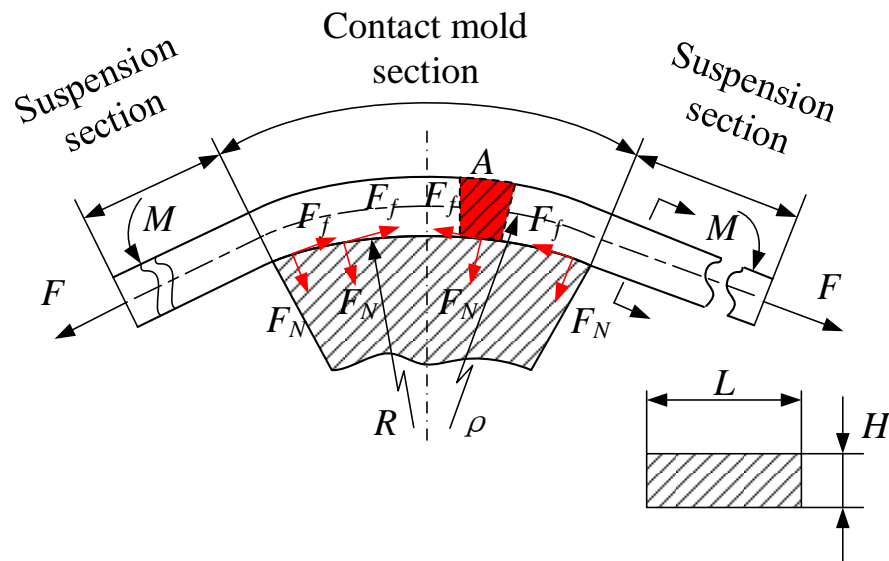
Figure 1. Force analysis of the stretch and bend synchronous loading process.

Due to the axial symmetry of the contact mold segment, 1/2 was taken for analysis. The contact mold segment was divided into innumerable micro-units. The force analysis of the micro-unit at section A point shown in Figure 1 was taken as shown in Figure 2. The arc angle corresponding to the micro-unit is $\Delta\theta$. The tension on the left and right sides of the micro-unit are F_{i+1} and F_i, respectively. The positive pressure of the micro-unit on the arc surface of the mold is F_{N_i}. According to the decomposition of forces and Coulomb's law of friction, the positive pressure F_{N_i} and the frictional force F_{f_i} on the surface of the micro-unit are calculated as:

$$F_{N_i} = F_i \sin \frac{\Delta\theta}{2} + F_{i+1} \sin \frac{\Delta\theta}{2} \tag{3}$$

$$F_{f_i} = \mu F_{N_i} = \mu(F_i \sin \frac{\Delta\theta}{2} + F_{i+1} \sin \frac{\Delta\theta}{2}) \tag{4}$$
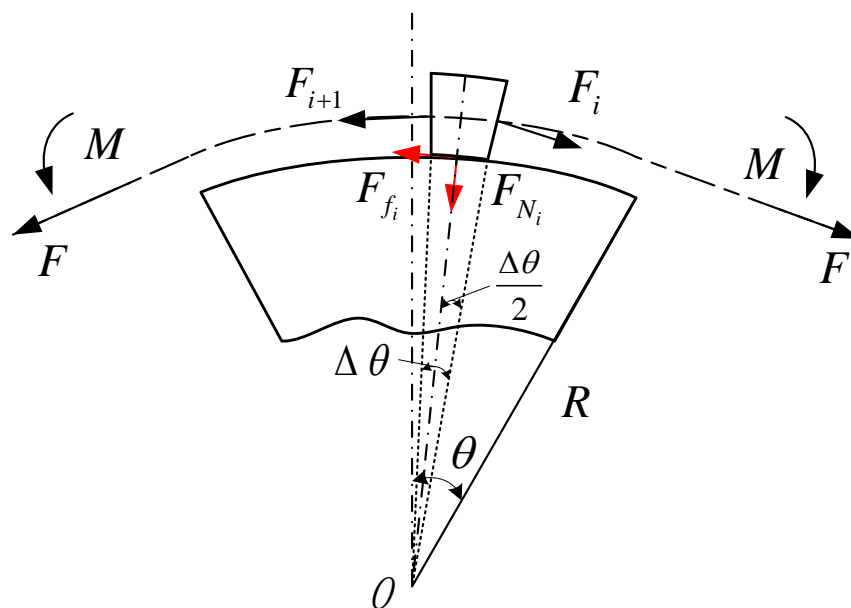

Figure 2. Force analysis of micro-unit at point A.

According to Newton's first law, the equilibrium equation of the tangential force of the i-th micro-unit in the direction of the length of the specimen contact mold segment is as:

$$F_{f_i} = F_i - F_{i+1} \tag{5}$$

Since $\Delta\theta$ is an infinitesimal quantity, there is $\sin\frac{\Delta\theta}{2} \approx \frac{\Delta\theta}{2}$. Take $F_1 = F$, and divide θ into n parts, $n \to \infty$. Equation (5) is brought into Equations (3) and (4), and the positive pressure F_{N_i}, friction force F_{f_i}, and tension force F_i of the i-th micro-unit are obtained by iterative collation, respectively.

$$F_{N_i} = 2\Delta\theta F \frac{(2 - \mu\Delta\theta)^{i-1}}{(2 + \mu\Delta\theta)^i} \tag{6}$$

$$F_{f_i} = 2\mu\Delta\theta F \frac{(2 - \mu\Delta\theta)^{(i-1)}}{(2 + \mu\Delta\theta)^i} \tag{7}$$

$$F_i = F \frac{(2 - \mu\Delta\theta)^{(i-1)}}{(2 + \mu\Delta\theta)^{(i-1)}} \tag{8}$$

As shown in Figure 2, the contact area between the micro-unit and the arc surface of the mold is $S = R\theta L$. According to the formula of shear stress $\sigma = F/S$, the frictional shear stress τ_{f_i} and tensile stress τ_i of the i-th micro-unit can be obtained as follows:

$$\tau_{f_i} = 2\mu\Delta\theta F \frac{(2 - \mu\Delta\theta)^{(i-1)}}{(2 + \mu\Delta\theta)^i R\Delta\theta L} \tag{9}$$

$$\tau_i = F \frac{(2 - \mu\Delta\theta)^{(i-1)}}{(2 + \mu\Delta\theta)^{(i-1)} R\Delta\theta L} \tag{10}$$

The parameters of the stretch-bend as shown in Table 1 are brought into Equations (9) and (10). The variation curves of the frictional shear stress and the total tensile stress in the cross-section for each micro-unit in the contact mold segment of the specimen were obtained by numerical calculation, as shown in Figures 3 and 4.

Table 1. Stretch-bend parameters.

| Tension F/kN	Bend Angle θ/°	Friction Coefficients μ	Bending Radius R/mm	Section Width L/mm
30	30	0.15, 0.2, 0.25	150	20
30	30, 45, 60	0.2	150	20

It can be seen from Figure 3 that the rightmost micro-unit is subjected to frictional shear stresses of 0.599, 0.799, and 0.99 MPa, respectively, when the friction coefficients of contact sections are 0.15, 0.2, and 0.25, respectively. The normal pressure of the micro-unit from right to left gradually decreases, resulting in a lower frictional force on the micro-unit at the same friction coefficient. As the friction coefficient increases, the frictional shear stress on the micro-unit at the same position becomes larger. It is known that the magnitude of the frictional shear stress of the micro-unit is related to the friction coefficient and the position of the micro-unit. That is, the smaller the coefficient of friction, the farther the location of the micro-unit from the point of tension is, and the smaller the frictional shear stress on the micro-unit is.
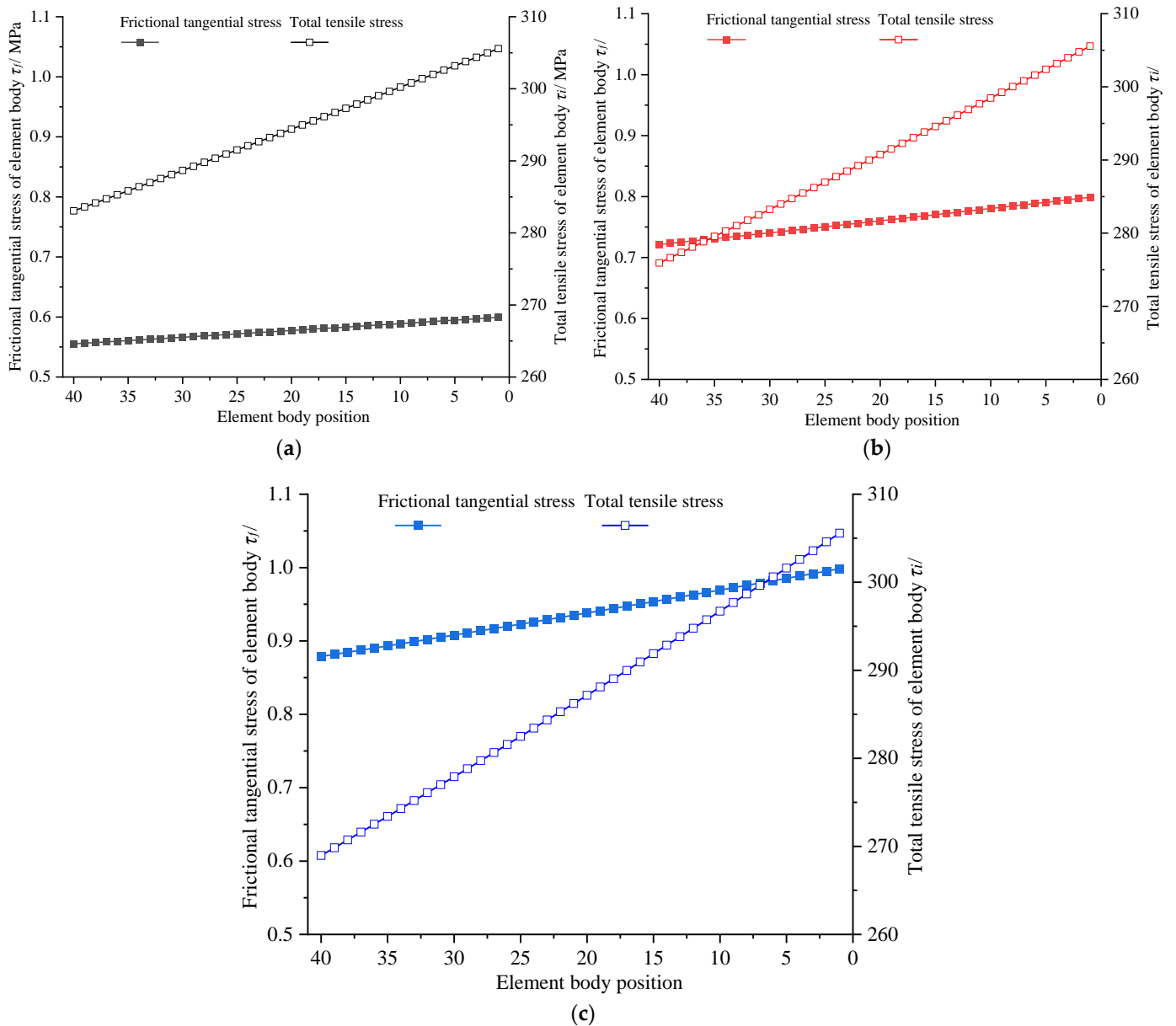
Figure 3. The frictional tangential stress and total tensile stress of each micro-unit under different friction coefficients. (**a**) $\mu = 0.15$; (**b**) $\mu = 0.2$; (**c**) $\mu = 0.2$.

It can be seen from Figure 3 that the total tensile stress on the rightmost micro-unit for all three friction coefficients was 305.577 MPa. From right to left along the direction of the bending arc, the total tensile stress experienced by the micro-unit showed a significant decrease. Since the order of frictional shear stress is much smaller than the tensile stress in the micro-unit cross-section, it is known from Equation (5) that the tensile stress in the micro-unit was $F_{i+1} = F_i - F_{f_i}$. The superimposed accumulation of frictional shear stress makes the tensile stress in the bending specimen unevenly distributed.

It can be seen from Figure 4 that under different bending angles, the varying trends of the frictional shear stress and total tensile stress of the micro-unit were the same, decreasing in turn along the arc direction of the specimen from right to left. The larger the bending angle of the specimen, the smaller the frictional shear stress and the total tensile stress of the micro-units farthest from the point of action of the tensile force are, and the more obvious the uneven stress distribution on the left and right sides of the specimen.
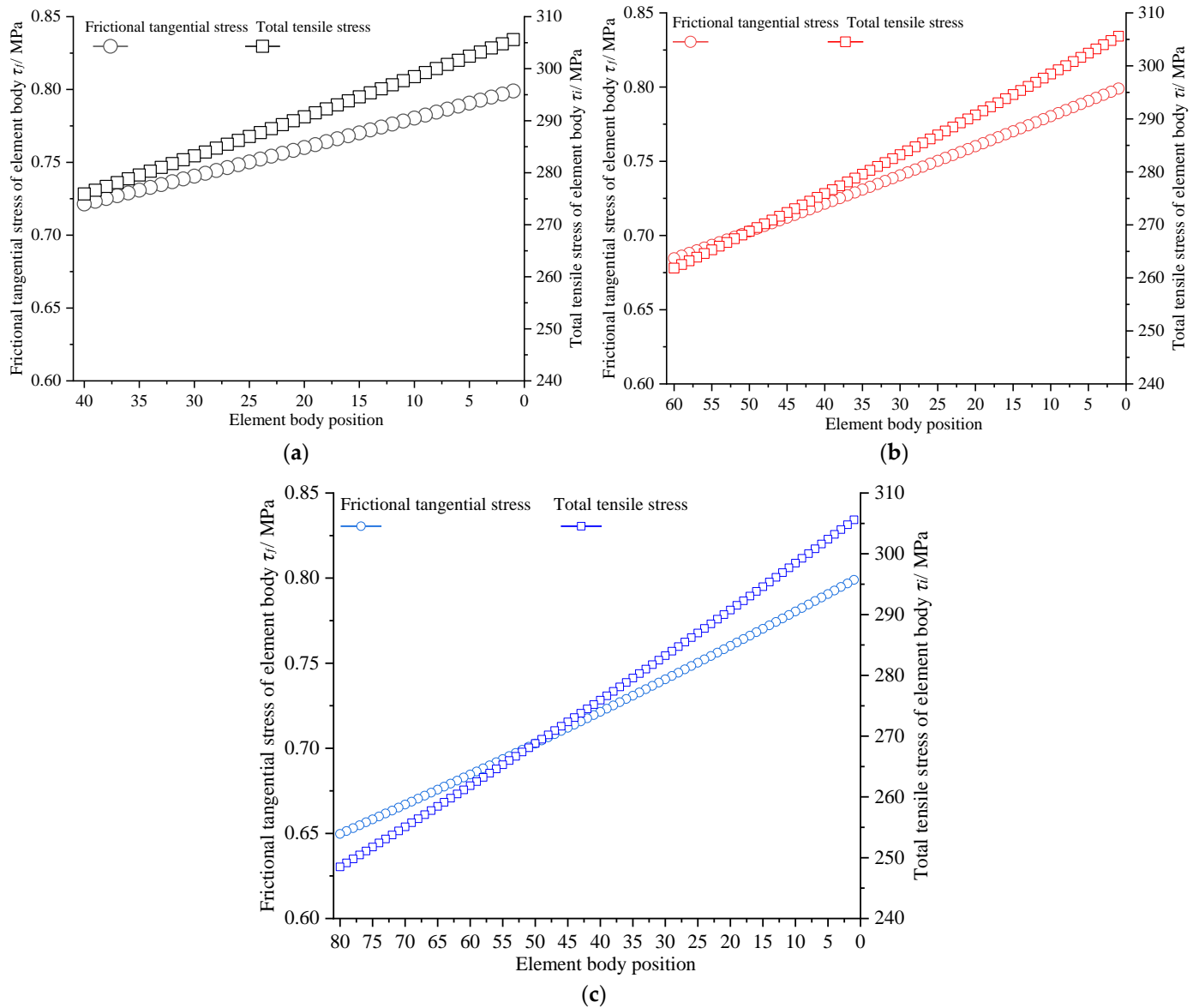
Figure 4. The frictional tangential stress and total tensile stress of each element under different bend angles. (**a**) 30° contact mold; (**b**) 45° contact mold; (**c**) 60° contact mold.

2.2. Strain Distribution of Stretch-Bend Forming

It is assumed that the material enters the plastic deformation stage completely during the stretch-bend forming process. A bilinear hardening power exponential strengthening model [29] was used to depict the stress–strain relationship during bending tensile loading.

$$\sigma = A + B\varepsilon_p{}^n \tag{11}$$

where, *A* is the initial yield strength of the material; *B* is the process-hardening modulus, which is the slope of the stress–strain curve in the plastic deformation stage; ε_p is the equivalent plastic strain; *n* is the strain-hardening index, which reflects the ability of the metal material to resist uniform plastic deformation.

Substituting Equation (11) into Equation (10), the plastic strain at the contact surface of the *i*-th micro-unit and the mold was obtained as follows.

$$\varepsilon_i = \left(\frac{F(2 - \mu\Delta\theta)^{(i-1)}}{(2 + \mu\Delta\theta)^{(i-1)}R\Delta\theta LB} - \frac{A}{B} \right)^{\frac{1}{n}} \tag{12}$$

The inner material fibers are compressive elastic–plastic deformation, while the outer material fibers are tensile elastic–plastic deformation under the action of the bending moment. The friction produces a shearing effect on the contact surface of the inner layer of the specimen, changing the stress–strain distribution of the cross-section. The stress–strain distribution of the profile cross-section under the action of frictional shear is shown in Figure 5. It can be seen from Figure 5 that the frictional shear stress on the surface of the profile in contact with the mold was the largest, and the frictional shear stress decreased in a gradient along the thickness direction of the profile on the section until the frictional shear stress on the upper surface of the profile approached zero. The tensile stress and strain on the upper surface of the profile were much greater than those on the lower surface.

(a) Bilinear hardening power exponential strengthening model

(b) Cross-sectional stress distribution
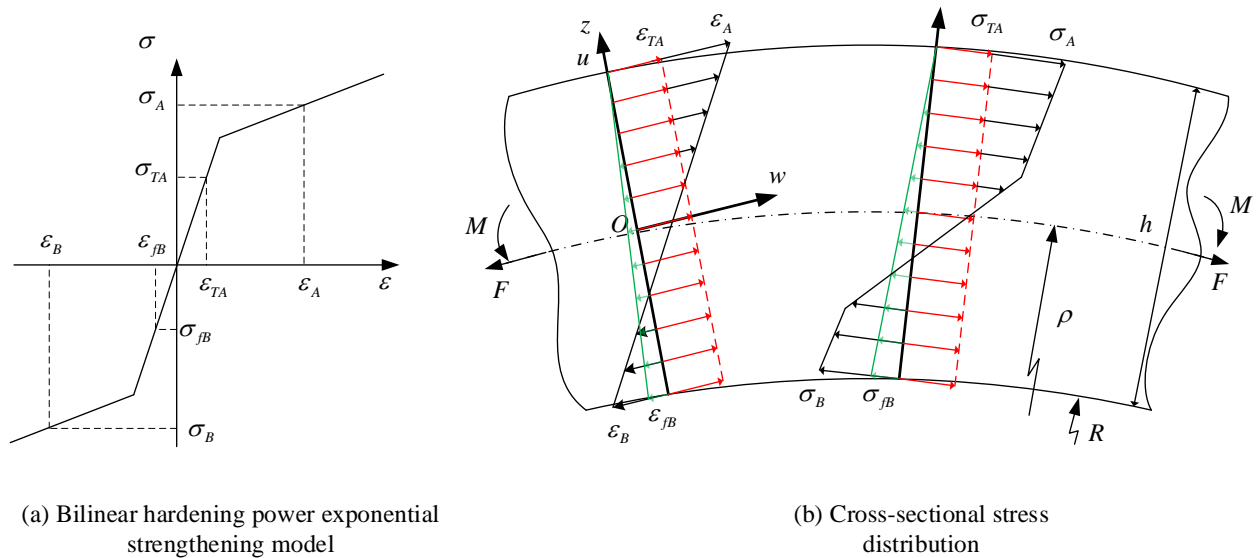
Figure 5. Stress–strain distribution of the stretch-bend section. (**a**) Bilinear hardening power exponential strengthening model; (**b**) cross-sectional stress distribution; where, *wou* is the neutral layer coordinate system; σ and ε are the total stress and total strain of the section, respectively; σ_A and ε_A are the total stress and total strain of the outermost layer of the section, respectively; σ_{fB} and ε_{fB} are the frictional shear stress and strain of the contact interface between the inner layer of the section and the mold, respectively; σ_B and ε_B are the total stress and total strain of the innermost fiber, respectively.

3. Aluminum Alloy Profile Simulated Stretch-Bend Experiment

The friction changes the stress and strain distribution within the stretch-bend forming specimen, which affects the forming load as well as the plastic deformation. In order to research the effect of friction of the contact interface on the plastic deformation of the stretch-bend forming specimen, the stretch and bend synchronous loading experiment was used to simulate the stretch-bend forming process of aluminum alloy profiles, and the influence of friction coefficient and contact mold angle on the section deformation and tensile deformation of the specimen was analyzed.

3.1. Experiment Specimen

The experimental material in this study is AL6005A-T6 aluminum alloy profile with the chemical composition shown in Table 2.

Table 2. Chemical composition of Al6005A-T6 aluminum alloy profiles (%, mass fraction).

Si	Mg	Fe	Cu	Mn	Cr	Ti	Zn
0.5–0.9	0.4–0.7	0.35	0.3	0.5	0.3	0.1	0.2

According to the international standard ISO 6892-1-2019 [30], metal material tensile experiment standard at room temperature, in the INSTRON 5982 electronic universal material testing machine by INSTRON CORPORATION of located in Boston, MA, USA for the uniaxial tensile experiment, the load measurement accuracy of the testing machine is not less than ±0.4%, and the movement accuracy error is ±0.0001 mm. The loading rate is 3 mm/ min, and the specimen specifications are 20 mm × 5 mm × 200 mm. We repeated the uniaxial tensile experiment three times and took the average value. Finally, the mechanical property parameters of the experiment aluminum alloy profile specimens are shown in Table 3. The static tensile material engineering stress–strain curves of the specimens are shown in Figure 6.

Table 3. Tensile mechanical properties of Al6005A-T6 aluminum alloy profiles.

| Extension Percentage/%	Yield Strength/MPa	Tensile Strength/MPa	Elastic Modulus/GPa	Poisson Ratio	Tension Rupture/kN
17	282.2 ± 1.1288	300.5 ± 1.202	66.77 ± 0.26708	0.3	29.53 ± 0.11812
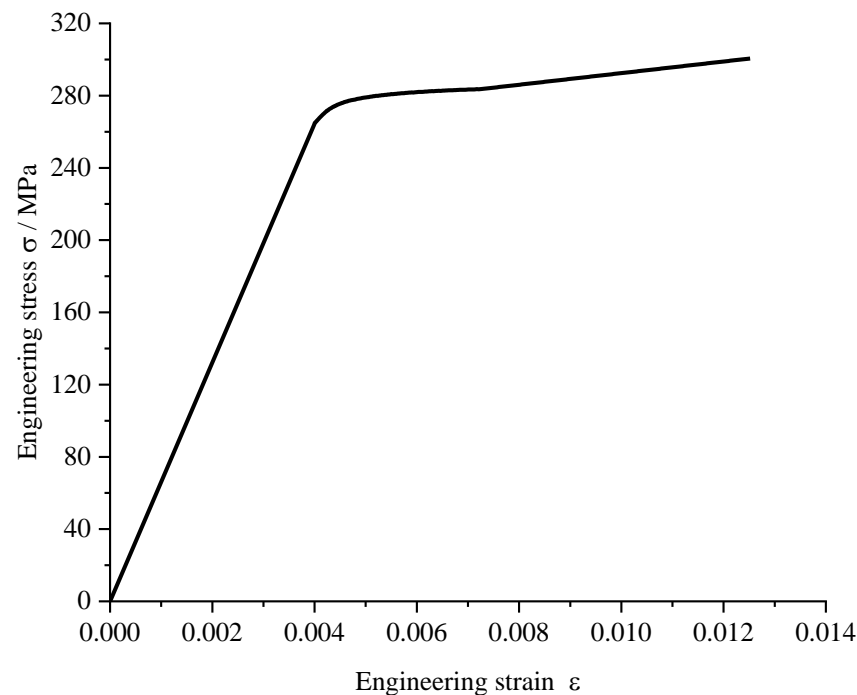
Figure 6. Engineering stress–strain curve of AL6005A-T6 aluminum alloy profile.

To explore the plastic deformation during the simultaneous tensile-bending loading phase, combined with the mechanical properties of the experiment specimen, we ensured that the specimen entered the plastic deformation stage and was not pulled off. Three types of stretch-bend specimens were made according to the different contact mold angles, as shown in Table 4. To analyze the strain variation of the specimen in the length direction, the specimen needs to be pre-treated as follows: (1) a flexible film is sprayed on the upper surface of the specimen, and no flexible film is sprayed on the down surface; (2) the strain measurement grid lines with 2 mm spacing were laser engraved in the deformation area of the specimen to form a strained grid as shown in Figure 7. The laser-engraved strain grid lines are of high accuracy and consistency while not damaging to the specimen itself. Since the flexible film can plastically deform and elongate synchronously with the specimen, the deformation amount of the specimen strain element can be obtained by measuring the grid width of the flexible film after laser engraving.

Table 4. Specimen sizes at different contact mold angles.

Contact Mold Angle $\theta/°$	Specimen Length L/mm	Contact Mold Length L_1/mm	Suspension Length L_2/mm	Clamping Length L_4/mm	Section Width B/mm	Section Thickness H/mm
30	280 ± 0.01	80	100	100	20 ± 0.01	5 ± 0.01
45	320 ± 0.01	120	100	100	20 ± 0.01	5 ± 0.01
60	360 ± 0.01	160	100	100	20 ± 0.01	5 ± 0.01

(a)

(b)

(c)
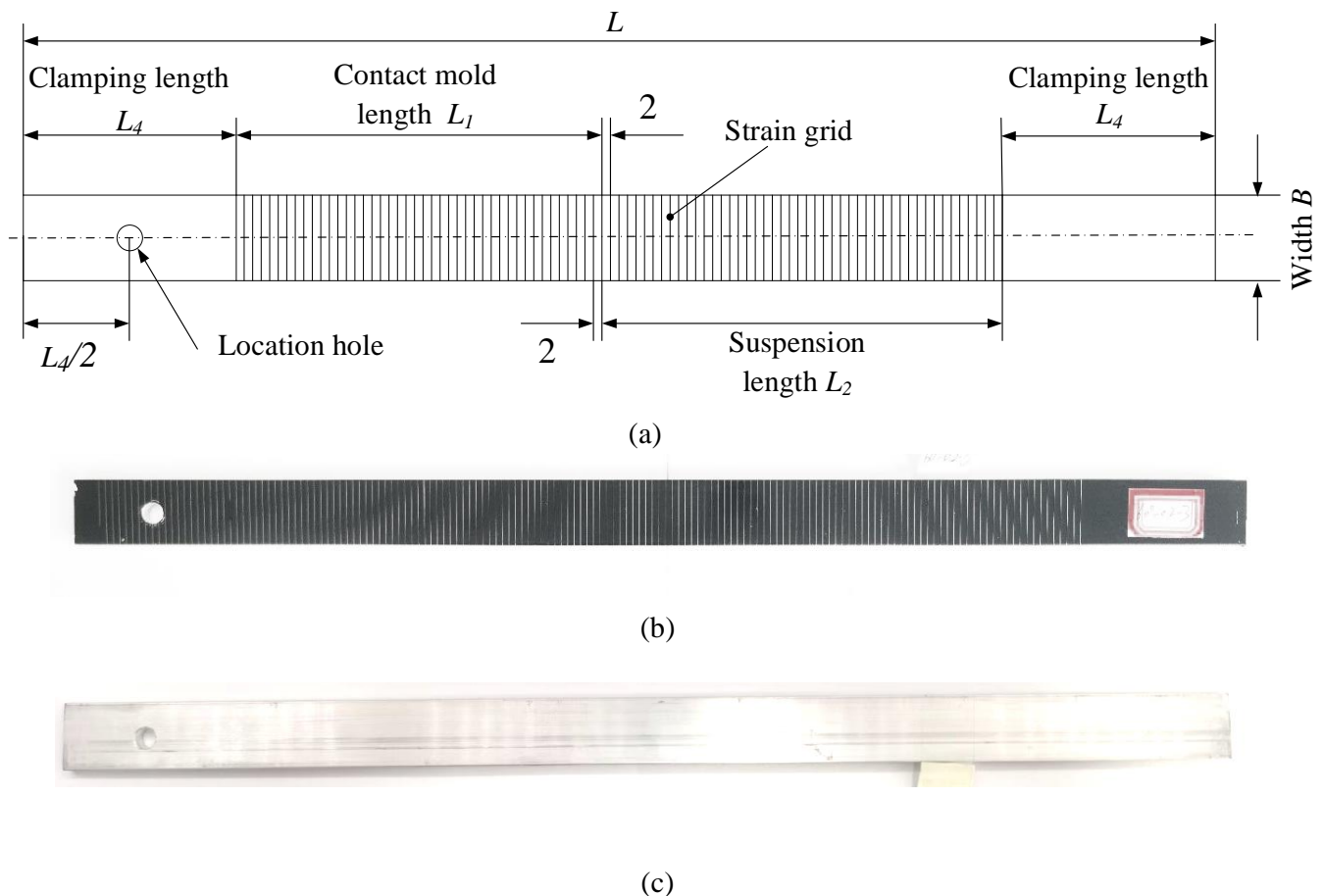
Figure 7. Structure size of the specimen. (**a**) Specimen size; (**b**) Upper surface of test sample; (**c**) Down surface of test sample.

3.2. Equipment and Methods of the Equivalent Stretch-Bend Experiment

To further analyze the effects of contact friction and contact mold angle on plastic deformation of stretch-bend specimens, the equivalent stretch-bend experiment was carried out on the tensile testing machine by auxiliary tooling. The equipment of the equivalent stretch-bend experiment is mainly composed of the main body of the stretch-bend mold, replaceable upper clamp, bending limit roller, fixed block, and other parts, as shown in Figure 8. The replaceable clamp and bending limit rollers can be used at the same time to achieve three types of contact mold angle of bending experiments as shown in Figure 8. The suspension section and the tensile axis of the specimen were ensured to be in the same straight line.

(a) 30° contact mold　　　　(b) 45° contact mold　　　　(c) 60° contact mold
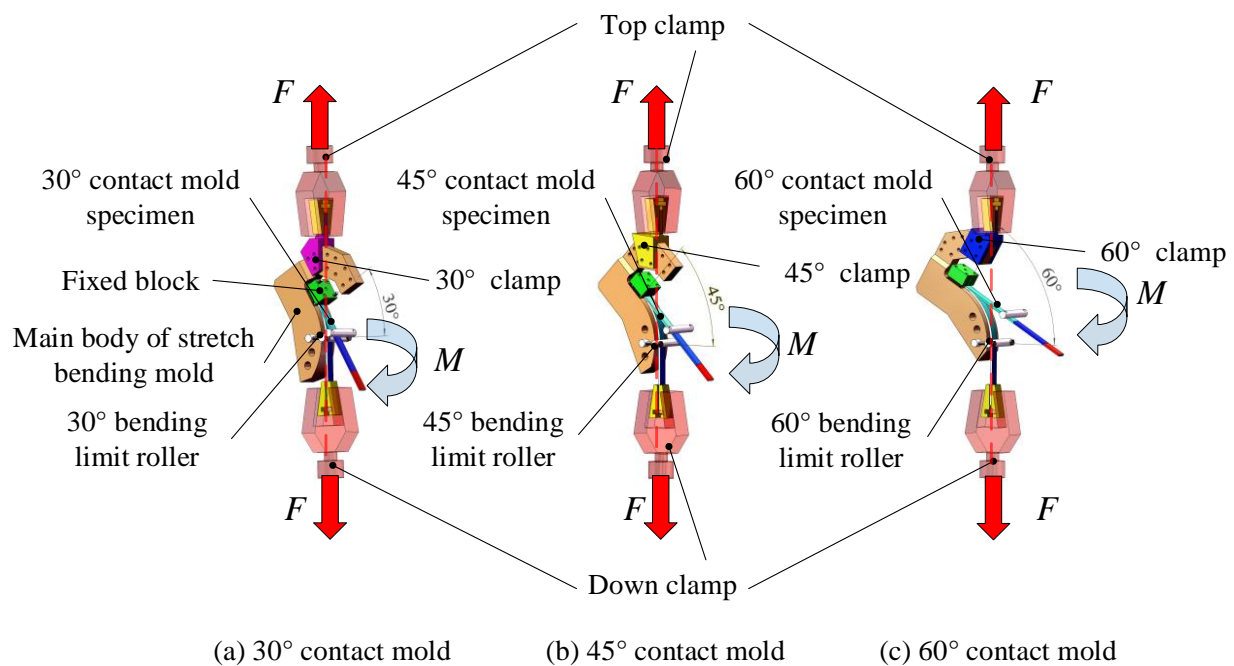
Figure 8. Equipment and methods of the equivalent stretch-bend experiment.

The specific method of the equivalent stretch-bend experiment is as follows: (1) The upper end of the specimen is fixed to the main body of the stretch-bend mold by the fixing block and limit pin. The bending moment M is applied to the specimen as shown in Figure 8 to make the specimen fit on the stretch-bend mold. (2) Lock the bending limit roller to press the specimen onto the stretch-bend mold. (3) Adjust the upper and lower clamps of the INSTRON 5982 electronic universal material test machine to intersect at 90°. The replaceable upper clamp of the stretch-bend experiment equipment and the lower end of the tensile specimen are respectively installed in the upper and lower clamps of the tensile experimental machine and locked. (4) Apply 2 kN pre-tension to the specimen, and then open the bending limit roller. The specimen is kept on bending contact with the mold under pre-tension. (5) The displacement control method is used for tensioning with a loading speed of 3 mm/min and a strain rate of 0.115 s^{-1}. Figure 9 shows the equivalent stretch-bend experiment of 30° contact mold. Repeat steps (1)–(5) for 30°, 45°, and 60° equivalent stretch-bending experiments, respectively. According to the mechanical properties of the material, the tensile-bending specimens are ensured to enter the plastic deformation stage. The tensile amounts of the specimens with different contact mold angles are determined by the equal tensile proportion, and the tensile amount is rounded off. Finally, the tensile rates of 30°, 45°, and 60° contact mold were 4.29%, 4.37%, and 4.44%, respectively. The specific experiment plan is shown in Table 5. As Bhanudas Bachchhav et al. [31] carried out sliding friction experiments with different surface roughness, the research results showed that the rougher the surface, the greater the friction coefficient. Zhang et al. [32] pointed out that when the surface roughness Ra of the mold was 1.6 um, the friction coefficient between the test specimen and the mold was 0.21 in the study of the influence of low-frequency vibration on the friction coefficient of the stretch-bend. Based on the abovementioned relationship between surface roughness and friction coefficient, in this experiment, equivalent stretch-bend experiments were carried out with molds with roughness Ra of 6.3 and 12.5, respectively, to simulate the equivalent stretch-bend forming under two different contact interface friction coefficients.

The specimen after stretch-bend is shown in Figure 10. The micrometer was used to measure the width of the upper and lower edges of the three equal cross-sections $AA'DD'$, $BB'EE'$, and $CC'FF'$ of the specimen contact mold segment and the three equal cross-sections GG', HH', and II' of the specimen suspension segment. The measurement

accuracy of micrometer was ±0.001 mm. The strain grids of the contact mold segment and the suspension segment of the specimen were measured one by one in the tensile direction with a 40× light microscope, and the plastic deformation of the strain mesh was calculated. The measurement accuracy of optical microscope was ±0.001 mm. The measurement accuracy was less than an order of magnitude of plastic deformation, so the measurement error did not affect the analysis of plastic deformation results, and had certain credibility.
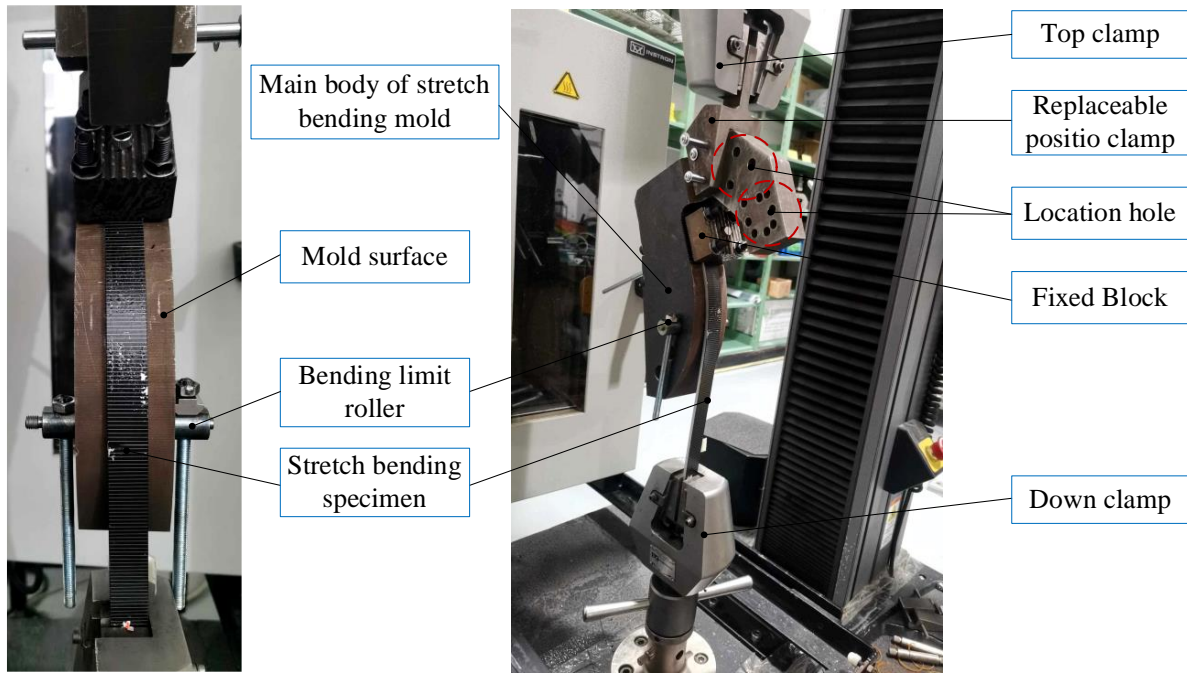
Figure 9. Equivalent stretch-bend experiment.

Table 5. The equivalent of the stretch-bend experiment parameters.

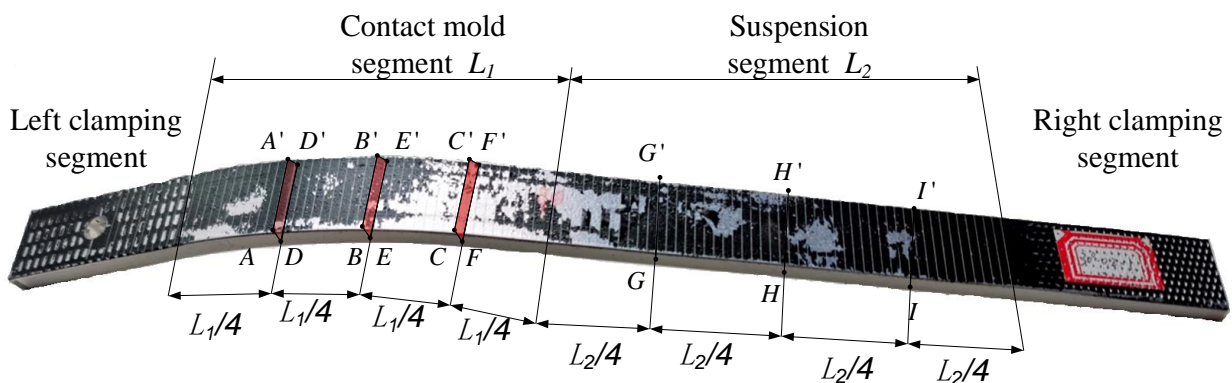| Condition	Mold Surface Roughness Ra/um	Contact Angle θ/°	Specimen Length L/mm	Stretching Value ΔL/mm
1	6.3	30	280 ± 0.01	12 ± 0.0001
2	12.5	30	280 ± 0.01	12 ± 0.0001
3	6.3	45	320 ± 0.01	14 ± 0.0001
4	12.5	45	320 ± 0.01	14 ± 0.0001
5	6.3	60	360 ± 0.01	16 ± 0.0001
6	12.5	60	360 ± 0.01	16 ± 0.0001

Figure 10. The specimen after stretch-bending.

4. Experiment Results and Analysis

4.1. Effect of Contact Interface Friction and Contact Mold Angle on Shrinkage Deformation of the Cross-Section

4.1.1. Cross-Section Shrinkage Deformation Analysis

Figure 11 shows the width change curve of the upper and lower edges of the specimen cross-section with a smooth mold stretch-bend. It can be seen from Figure 11 that with the 30° contact mold stretch-bend, the upper surface deformed widths of the contact mold segment $AA'DD'$, $BB'EE'$, and $CC'FF'$ cross-sections were 19.87, 19.64, and 19.62 mm, respectively, while the lower surface deformed widths were 19.95, 19.90, and 19.66 mm, respectively. In Figure 11, the deformed widths of the upper and lower surfaces of the left $AA'DD'$ cross-section were between 19.87 and 19.98 mm, and the deformed widths of the upper and lower surfaces of the rightmost $CC'FF'$ cross-section were between 19.58 and 19.2 mm. That is, the width of the upper surface of the specimen was smaller than the width of the lower surface at the same cross-section position of the contact mold segment, and the width of the section from left to right decreased gradually. It should be noted that the deformation of the upper surface was much larger than that of the lower surface in the stretch-bend forming process. The closer to the action point of the tensile force, the greater the overall deformation of the section is. There was no width difference between the upper and lower surfaces in the cross-section of the suspension segment. The width of the neutral layer cross-section can be used for characterization. However, due to the inhomogeneity of the material, there was a slight fluctuation in the width of each cross-section of the suspension segment.
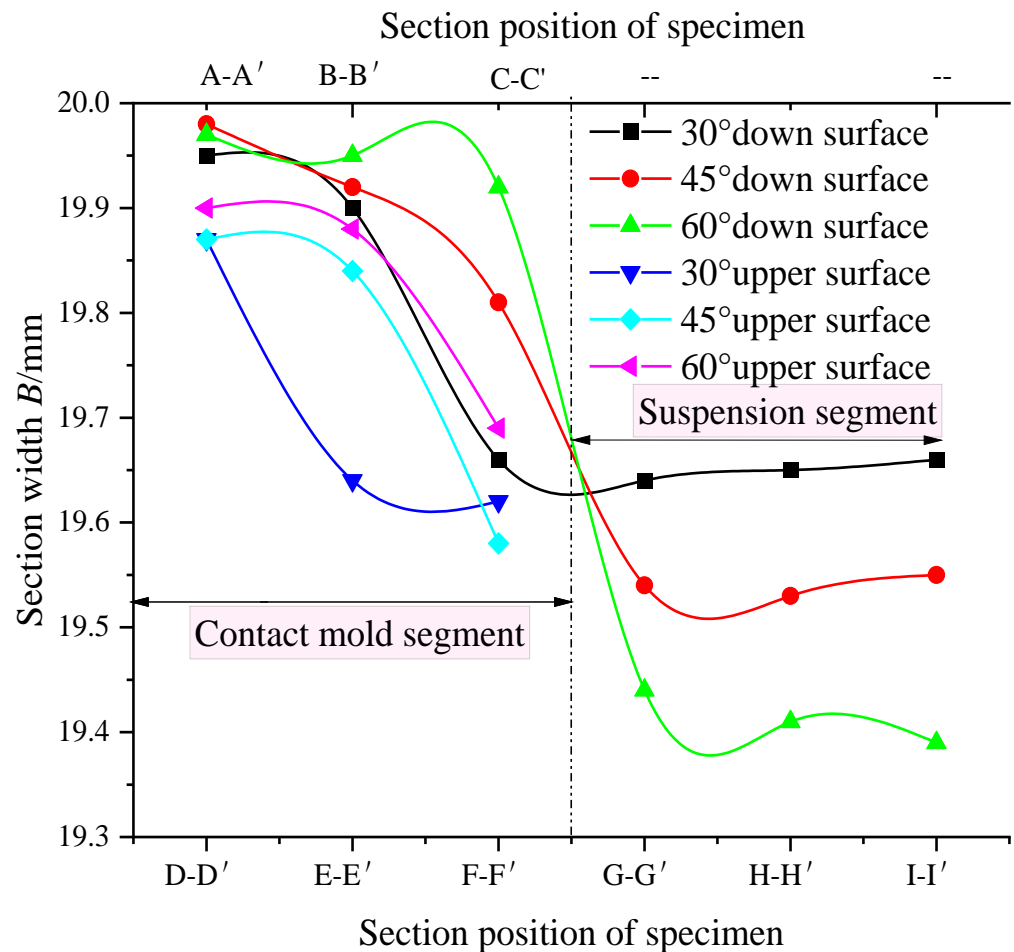

Figure 11. Variation curves of the upper and lower edges of the specimen cross-section with smooth die stretch-bending.

It can also be seen from Figure 11 that the cross-sectional width of the contact mold segment was between 19.58 and 19.98 mm, while the cross-sectional width of the suspension segment was between 19.39 and 19.66 mm. By taking the average of the three sampled section widths of the contact mold segment and analyzing the six sets of laboratory data, it can be seen that the cross-sectional deformation of the suspension segment was greater than that of the contact mold segment by more than 44.1%. With the increase of the contact mold angle, the plastic deformation of each cross-section of the contact mold segment decreased, while the plastic deformation of each cross-section of the suspension segment both had the opposite trend.

Figure 12 shows the average cross-sectional width of the contact mold segment and the suspension segment under the 45° contact mold and stretch-bend. The cross-section of the contact mold segment is a trapezoidal section with a width of 19.76 mm at the top bottom and 19.90 mm at the bottom. The cross-section of the suspension is a rectangular section with a width of 19.54 mm. It can be seen that the cross-sectional shapes of the contact mold segment and the suspension segment of the specimen are the scaled-down trapezoidal section and rectangular section, respectively, after stretch-bend plastic deformation with the rectangular sectional specimen according to the stress–strain distribution of the cross-section during the stretch-bend forming process shown in Figure 5. It is known that the tensile stresses of the contact mold segment are reduced due to the frictional forces of the contact interface and bending compressive stresses, which are distributed in a gradient in the thickness direction. The final result is that the plastic deformation of the upper surface is greater than the lower surface, and the cross-section of the contact mold segment is trapezoidal.
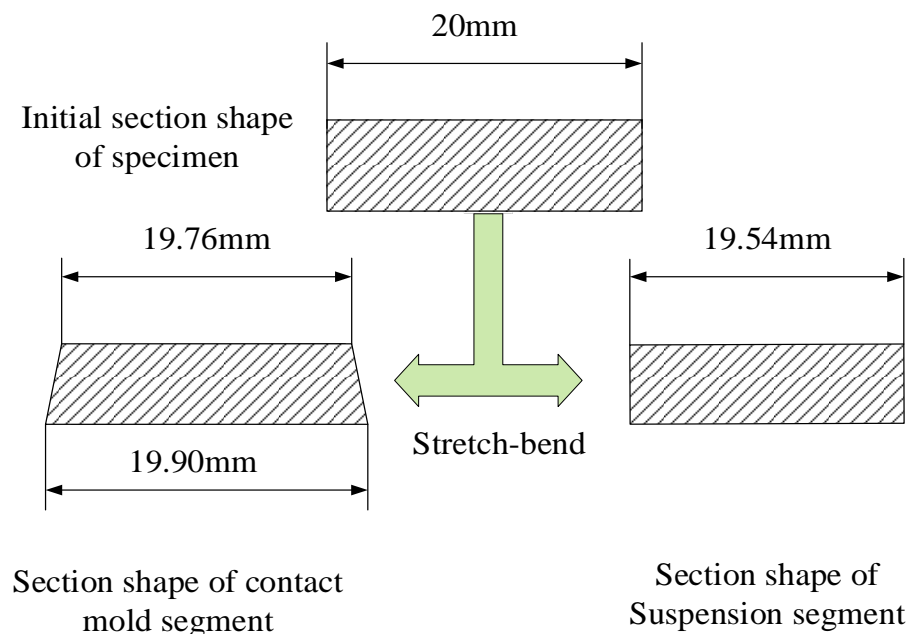

Figure 12. Deformation diagram of 45° contact mold stretch-bend sections.

4.1.2. Effect of Contact Interface Friction on Cross-Sectional Shrinkage Rate

The cross-section shrinkage rate is the ratio of the area of the cross-section in a reduction in the original cross-section area of the specimen under tensile plastic deformation, which is one of the plasticity indicators of the material. To further analyze the influence of contact interface friction on cross-section deformation of the contact mold segment, we calculated the shrinkage rate of each section according to the deformation shape of the specimen cross-section, as shown in Figure 12. Figure 13 shows the variation curve of the cross-section shrinkage rate of each section of the specimens with different roughness of the mold. It can be seen from Figure 13 that in the same contact mold angle, the smoother the contact surface, the smaller the friction coefficient is; then, the higher the section shrink-

age of the contact mold segment, the the lower the section shrinkages of the suspension segments are. In addition, the cross-section shrinkage of the contact mold segment was at most 4.45% of that of the suspension segment. This is mainly due to the improvement of the friction state and the reduction of the friction shear stress, which reduces the uneven distribution of tensile stress in the contact mold segment of the specimen.
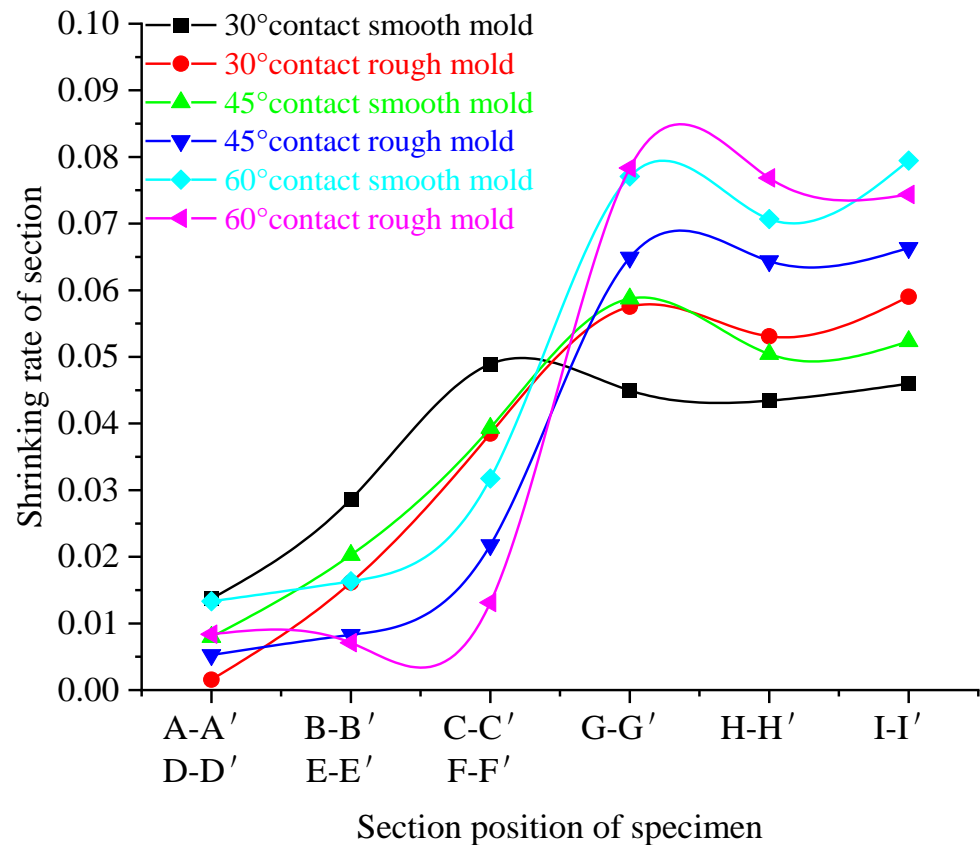

Figure 13. The variation curve of the cross-section shrinkage rate with different roughnesses of the mold.

4.1.3. Effect of Contact Mold Angle on Cross-Sectional Shrinkage Rate

The cross-sectional shrinkage rates of each section of the specimen contact mold segment and the suspension segment were averaged. The distribution of the cross-section shrinkage changes of both the specimen contact mold segment and the suspension segment under different contact mold angles is plotted as shown in Figure 14. It can be found from Figure 14 that with the contact mold angle of the specimen increased from 30° to 60°, the cross-section shrinkage rate in the contact mold segment of the smooth contact surface and rough contact surface decreased by 32.8% and 49.2%, respectively, and the cross-sectional shrinkage rate in the suspension segment increased by 60.7% and 35.3%, respectively. It can also be seen from Figure 14 that at 30°, 45°, and 60° contact mold angles, the smooth mold had an increase of 38.3%, 47.7%, and 53.4%, respectively, in the cross-sectional shrinkage rate of the contact mold segment compared with the rough mold. This is due to the increase of the contact mold angle of the specimen, making the total amount of friction resistance superposition in the contact mold segment become larger. As a result, the plastic deformation of the specimen contact mold segment was reduced, and the corresponding deformation of the suspension segment increased. The angle of the contact mold is inversely proportional to the shrinkage of the cross-section of the contact mold segment and positively proportional to the shrinkage of the suspension segment.
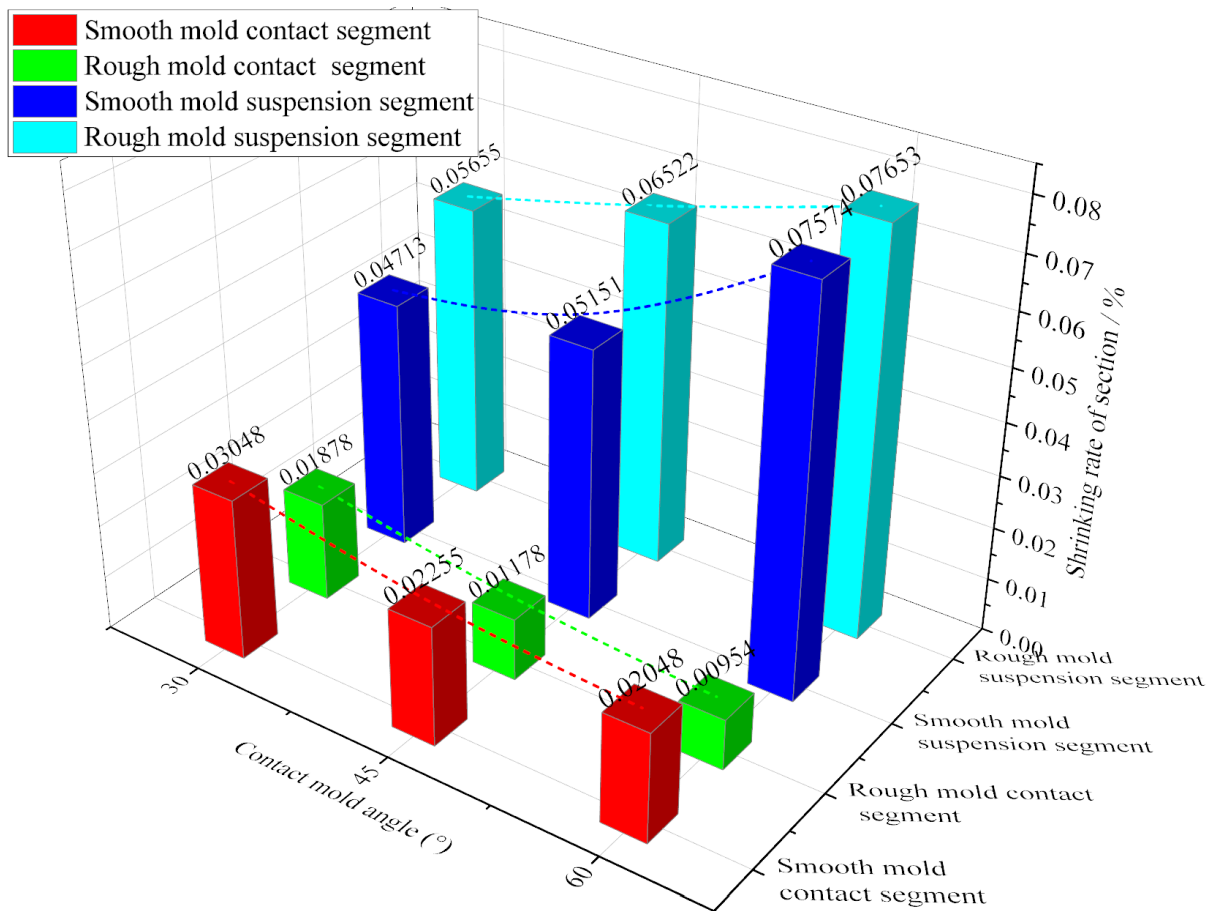
Figure 14. Cross-section shrinkage distribution of the contact mold segment and the suspension segment with different contact mold angles.

4.2. Effect of Contact Interface Friction and Contact Mold Angle on Tensile Deformation of the Cross-Section

4.2.1. Effect of Contact Interface Friction on Tensile Deformation of Contact Mold Segment

Figure 15 shows the strain grid length and deformation distributions of contact mold segments for 30°, 45°, and 60° of contact mold angle specimens under two types of mold surfaces. It can be seen from Figure 15b that the mesh deformation of the leftmost end micro-unit of the 45° contact mold specimen with smooth and rough contact surfaces was 0.025 and 0.02 mm, respectively. The micro-unit mesh deformation amounts were 0.097 and 0.06 mm, respectively. It can also be seen from Figure 15a–c that the mesh deformations of the micro-unit at both ends of the contact mold segment were not much different for stretch-bend the under different contact surfaces. However, the mesh deformation of the corresponding micro-unit in the middle of the contact mold segment for the smooth mold stretch-bend was much larger than that for the rough mold stretch-bend. The mesh deformation of the micro-unit in the contact mold segment increased in a gradient from left to right.

From Equations (9) and (10) and Figure 3, it can be seen that the frictional shear stress was gradually accumulated and superimposed along with the grid mesh from right to left, resulting in a gradient distribution of tensile stress, and the tensile stress of the leftmost element was the smallest. Therefore, the deformation elongation of the micro-unit at the left end measured by the experiment was much smaller than that at the right end. It can be seen from Figure 3 that the larger the friction coefficient of the contact interface, the faster the tensile stress of the micro-unit decreases, which leads to the greater the tensile deformation gradient of the micro-unit of the contact mold segment.
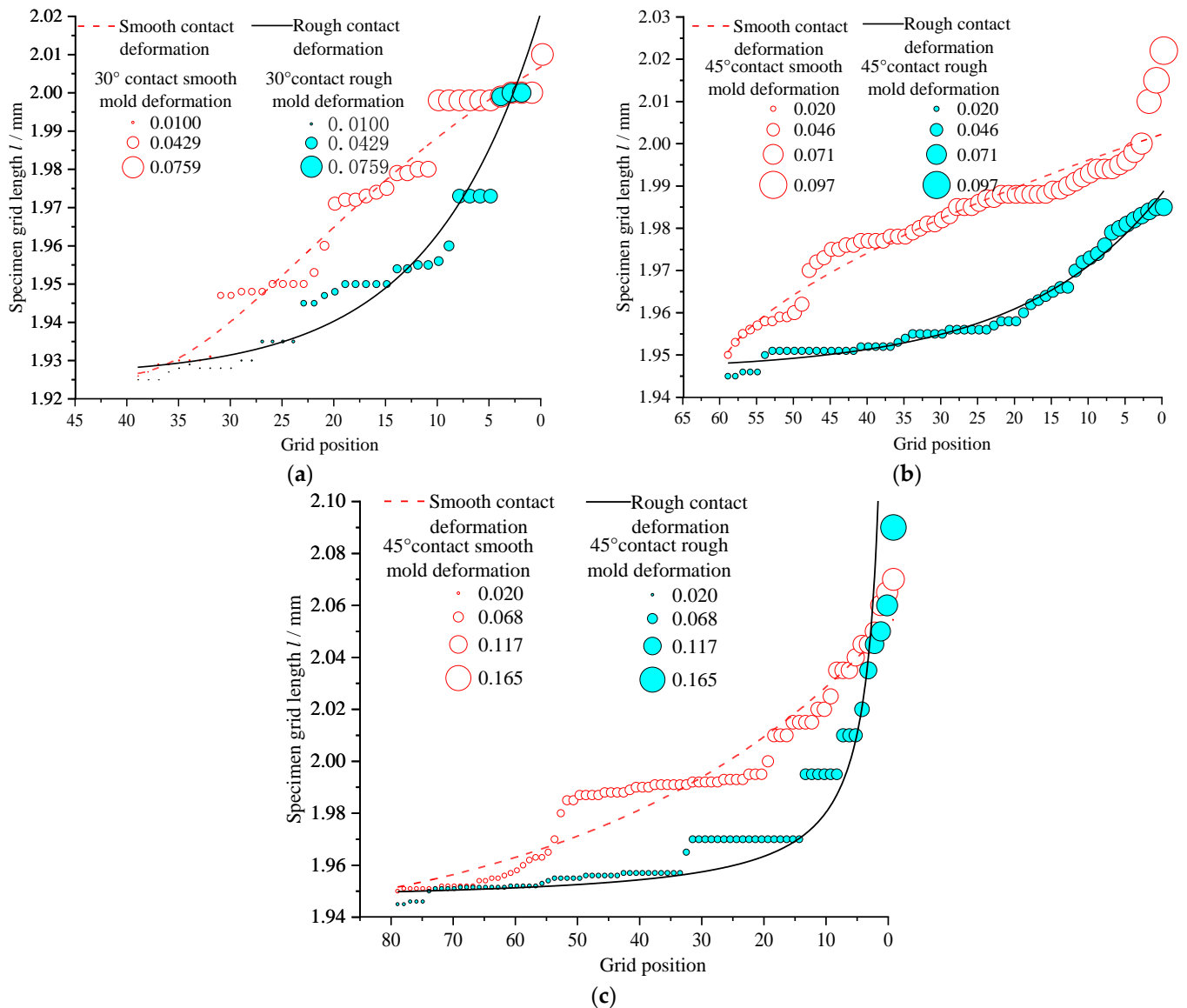
Figure 15. Strain grid length and deformation distribution of the contact mold segment. (**a**) 30°
contact mold angle; (**b**) 45° contact mold angle; (**c**) 60° contact mold angle.

There is a certain degree of fluctuation in the deformation of the strain mesh due to
measurement errors and the non-uniformity of the material. The strain mesh length in
Figure 15 was fitted by the least squares method. It could be found that the deformation
gradient of the smooth mold stretch-bend micro-unit mesh was smaller than that of the
rough mold by the fitting curve. That is, the rougher the stretch-bend mold is, the greater
the gradient of deformation of the contact mold segment is, and the worse the uniformity
of the formed specimen is.

The deformation of the strain grid of the 30-degree contact mold segment with rough-
ness Ra = 12.5 um in Figure 15a was extracted. According to the strain calculation formula,
the linear strain $\varepsilon_i = (l_i - l_0)/l_i$ of each strain element was calculated, where, l_i is the
length of strain grid after stretching, and l_0 is the length of strain grid before stretching. The
linear strain of each strain element of the contact mold segment was brought into the static
tensile stress–strain curve of the specimen material, and the tensile stress of each element
was obtained. The tensile stress of the micro-unit variation curve is plotted as shown in
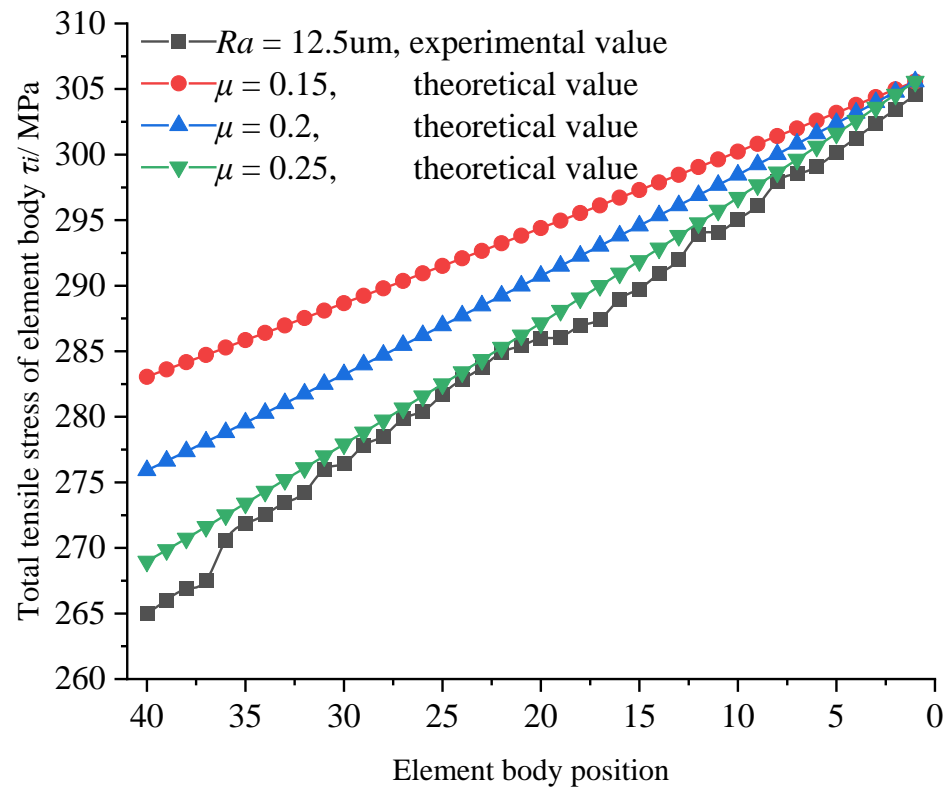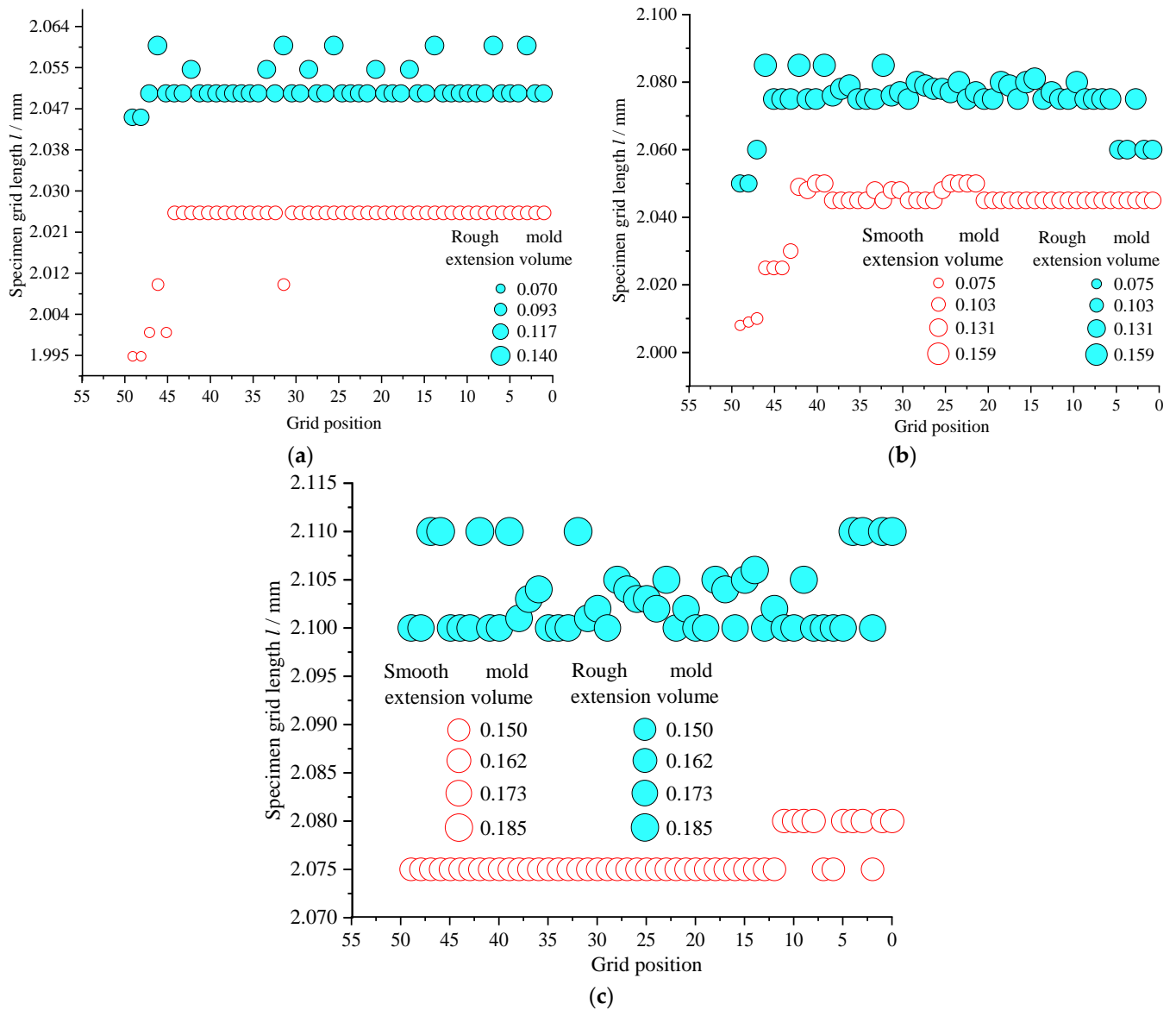Figure 16.

Figure 16. Variation curve of tensile stress.

It can be seen from Figure 16 that the tensile stress of the micro-unit by the experiment decreased from right to left along the specimen direction. When the mold surface roughness Ra was 12.5 um in the experiment and the contact interface friction coefficient μ was 0.25 in the theoretical derivation, the slope of the tensile stress gradient on the micro-unit was close to that. There were numerical fluctuations at individual measurement points, and the maximum error was 6.95 MPa. It can be seen that the experiment verified the gradient distribution law of the tensile stress on the micro-unit along the length of the specimen in the theoretical analysis. At the same time, it also indirectly indicated that the friction coefficient of the contact interface was close to 0.25 when the mold surface roughness was 12.5 um. The above provides a new method to obtain the friction coefficient of stretch-bend forming.

4.2.2. Effect of Contact Interface Friction on Tensile Deformation of the Suspension Segment

Figure 17 shows the strain grid length and deformation distribution of the suspension segment for 30°, 45°, and 60° contact mold angle specimens under two types of mold surfaces of the stretch-bend forming specimen. It can be seen from Figure 17a–c that there was a very small fluctuation in the mesh deformation of the micro-unit in the suspension segment of the specimen. Thereinto, the average deformation of the suspension segment micro-unit mesh for the 30° contact mold stretch-bend-formed specimen under two types of mold surfaces was 0.097 and 0.126 mm, respectively; the average deformation of the suspension segment micro-unit mesh for the 45° contact mold specimen was 0.116 and 0.149 mm, respectively; the average deformation for the 60° contact mold specimen was 0.150 and 0.178 mm, respectively.

Figure 17. Strain grid length and deformation distribution of suspension segment. (**a**) 30° contact mold; (**b**) 45° contact mold; (**c**) 60° contact mold.

It can be found that the smoother the contact surface, the smaller the tensile deformation of the suspension segment is, which is opposite to the tensile deformation of the contact mold segment in Figure 15. This is because the total amount of tensile displacement of the specimen as a continuous deformed body remains constant during the stretch-bend forming process. The friction force hinders the tensile plastic deformation of the contact mold segment, and the deformation of the suspension segment must increase to compensate for the reduced deformation of the contact mold segment.

4.2.3. Effect of Contact Mold Angle on Tensile Elongation

The elongation of the strain mesh of the micro-unit in the contact segment and the suspension of the specimen were counted, respectively. The tensile elongation distribution of the contact mold segment and the suspension segment with different contact mold angles was plotted as shown in Figure 18. It can be seen from Figure 18 that with the contact mold angle of the specimen increasing from 30° to 60°, the elongation of the contact mold segment of the smooth contact surface and rough contact surface decreased by 39.9% and 45.3%, respectively, and the elongation of the suspension segment increased by 55.2% and

40.8%, respectively. It can also be seen from Figure 14 that at 30°, 45°, and 60° contact mold angles, the smooth mold had an increase of 32.3%, 36.1%, and 38.3%, respectively in the elongation of the contact mold segment compared with the rough mold.
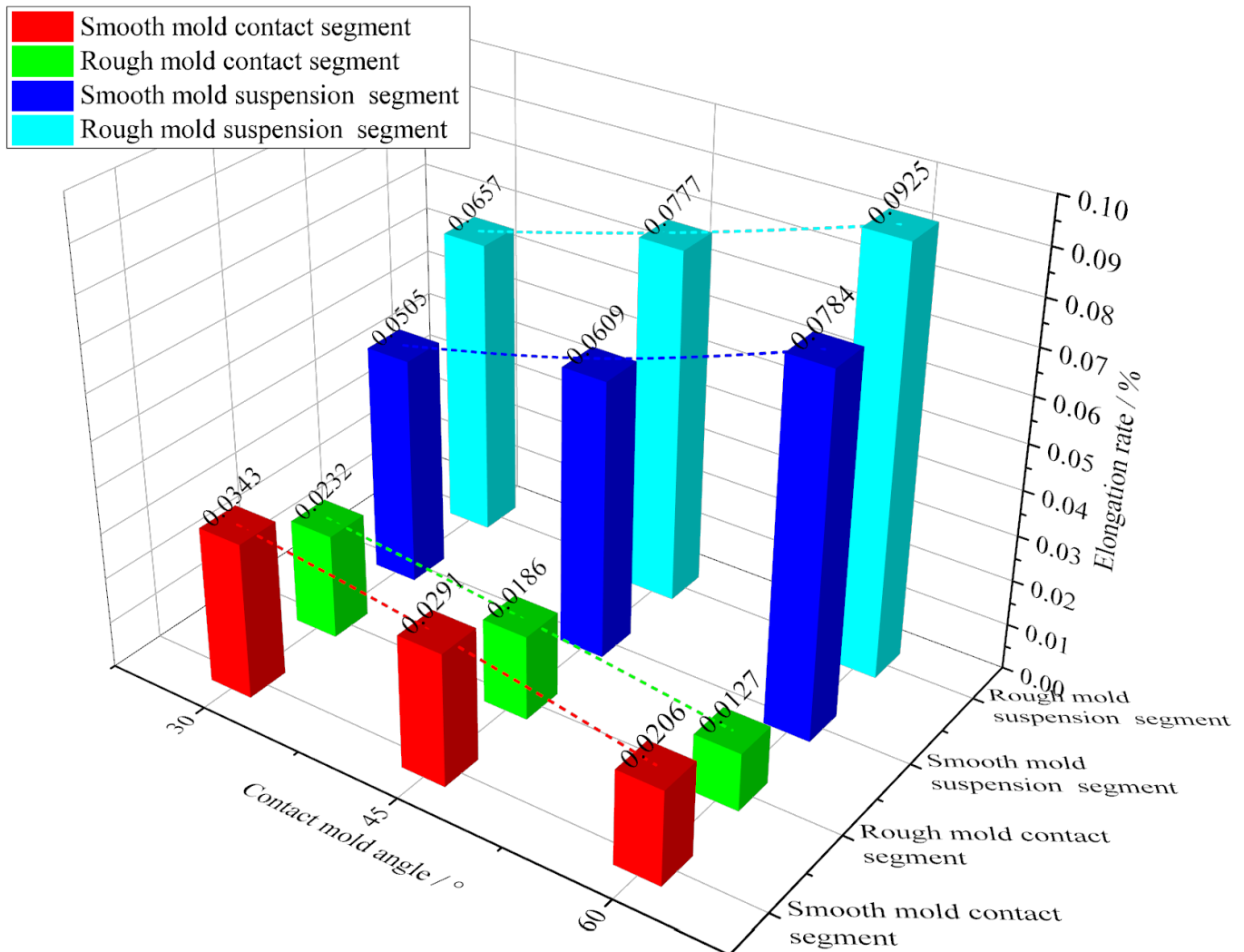
Figure 18. The tensile elongation distribution of the contact mold segment and the suspension segment with different contact mold angle.

According to the changes of frictional tangential stress and total tensile stress of each element under different bend angles, shown in Figure 4, the change gradient of the tensile stress of the micro-unit at the same position of the specimens with different contact mold lengths is the same. Due to the increase of the contact mold segment angle, the contact mold length between the specimen and the mold increased. The tensile stress of the more micro-units continued to decrease, which would lead to a decrease in the overall elongation of the die section. Therefore, with the increase of the contact mold angle, the elongation of the specimen contact mold segment decreases, and the elongation rate of the suspension segment increases. To improve the uniformity of the stretch-bend specimen, the bending contact mold angle of each loading step can be reduced to control the cross-section shrinkage and tensile elongation.

5. Conclusions

In this paper, the frictional plastic deformation behavior of the contact cross-section in the stretch-bend forming process was investigated. The analytical model of stress–strain distribution in the contact mold segment of stretch-bend forming was established by

element discretization. The effects of contact section friction state and contact interface angle on the cross-sectional shrinkage deformation, tensile deformation gradient of stretch-bend specimens, and deformation distribution were discussed by an equivalent stretch-bend forming experiment. Through theoretical derivation and equivalent experiments, some conclusions can be summarized as follows:

(1) The frictional shear stress of the discrete units in the contact mold segment was opposite to the tensile stress, and the cumulative superposition in the length direction of the specimen caused the uneven distribution of tensile stress. Generally, the larger the friction coefficient, the farther the micro-unit is away from the action point and the smaller the tensile stress on the micro-unit.

(2) The tensile stress of the contact mold segment gradually decreased from top to bottom along the thickness direction. The plastic deformation of the upper surface was greater than that of the lower surface, and the cross-section shape of the contact mold segment after stretch-bend forming was a trapezoid. The tensile stress and strain in the cross-section of the contact mold segment of the stretch-bend specimen were distributed in a trapezoid shape the cross-section, and the plastic deformation of the upper surface of the section was larger than that on the lower surface. As a result, the cross-section shape of the contact mold segment was trapezoidal after stretch-bend forming.

(3) In terms of the stretch-bend of the smooth mold compared with the rough mold, the cross-section shrinkage of the contact mold segment increased by more than 38.2%, and the elongation of the contact mold segment increased by more than 32.3%. The greatest effective factor of the specimen plastic deformation is the friction state of the contact interface. Generally, the better the friction state of the contact interface, the higher the cross-sectional shrinkage and elongation of the contact mold segment, and the smaller the tensile deformation gradient, and the smaller the cross-section shrinkage and elongation of the suspension segment. In order to improve the plastic deformation uniformity of the contact mold segment, the mold surface can be properly treated to reduce the friction coefficient.

(4) When the contact mold angle increased from 30° to 60°, the cross-section shrinkage of the contact mold segment decreased by more than 32.8%, and the elongation of the contact mold segment decreased by more than 39.9%. With the increase of the contact mold angle, the total amount of frictional shear stress and the tensile stress difference of both sides increased, the cross-section shrinkage and elongation of the contact mold segment decreased, and the cross-section shrinkage and elongation of the suspension segment increased. Therefore, reducing the angle of the contact mold can effectively control the influence of friction shear stress on plastic deformation.

References

1. Xiong, J.; Shen, Z. Rise and future development of Chinese high-speed railway. *J. Traffic Transp. Eng.* **2021**, *21*, 6–29. [CrossRef]
2. Ding, S.; Chen, D.; Liu, J. Research development and prospect of China high-speed train. *Chin. J. Theor. Appl. Mech.* **2021**, *53*, 35–50. [CrossRef]
3. Xu, H.; Liu, M.; Guo, Z.; Zou, Y.; Lu, R.; Gu, Z.; Cheng, X. Accuracy control of stretch bending for variable curvature L-section aluminum alloy door column of EMU. *J. Harbin Inst. Technol.* **2021**, *53*, 77–83. [CrossRef]
4. Zhai, R.; Ding, X.; Yu, S.; Wang, C. Stretch bending and springback of profile in the loading method of prebending and tension. *Int. J. Mech. Sci.* **2018**, *144*, 746–764. [CrossRef]
5. Xiang, N.; Shu, Y.; Wang, P.; Huang, T.; Guo, X.; Guo, J.; Chen, X.; Chen, F. Improved forming accuracy through controlling localized sheet metal deformation in the friction-assisted stretch bending process. *Int. J. Adv. Manuf. Technol.* **2021**, *116*, 3635–3650. [CrossRef]
6. Ma, J.; Welo, T.; Blindheim, J.; Ha, T. Effect of Stretching on Springback in Rotary Stretch Bending of Aluminium Alloy Profiles. *Key Eng. Mater.* **2021**, *883*, 175–180. [CrossRef]
7. Welo, T.; Ma, J.; Blindheim, J.; Ha, T.; Ringen, G. Flexible 3D stretch bending of aluminium alloy profiles: An experimental and numerical study. *Procedia Manuf.* **2020**, *50*, 37–44. [CrossRef]
8. Liang, J.; Liao, Y.; Li, Y.; Liang, C. Study on the Influence of Bending Angle of Multipoint Stretch-Bending of Profiles on Section Distortion of Parts. *Math. Probl. Eng.* **2020**, *2020*, 1975805. [CrossRef]
9. Chen, C.; Liang, J.; Li, Y.; Liang, C.; Jin, W. Springback Analysis of Flexible Stretch Bending of Multi-Point Roller Dies Process for Y-Profile under Different Process Parameters. *Metals* **2021**, *11*, 646. [CrossRef]
10. Liu, T.; Wang, Y.; Wu, J.; Xia, X.; Wang, J.; Wang, W.; Wang, S. Springback analysis of Z & T-section 2196-T8511 and 2099-T83 Al–Li alloys extrusions in displacement controlled cold stretch bending. *J. Mater. Process. Technol.* **2015**, *225*, 295–309. [CrossRef]
11. Liu, C.-G.; Zhang, X.-G.; Wu, X.-T.; Zheng, Y. Optimization of post-stretching elongation in stretch bending of aluminum hollow profile. *Int. J. Adv. Manuf. Technol.* **2015**, *82*, 1737–1746. [CrossRef]
12. Liu, B.; Cao, F.; Zeng, Y.; Wu, W. Numerical and experimental study on temperature and springback control of U-shape titanium extrusion hot stretch bending. *Int. J. Light. Mater. Manuf.* **2022**, *5*, 453–469. [CrossRef]
13. Ma, J.; Welo, T. Analytical springback assessment in flexible stretch bending of complex shapes. *Int. J. Mach. Tools Manuf.* **2020**, *160*, 103653. [CrossRef]
14. Maati, A.; Tabourot, L.; Balland, P.; Ouakdi, E.; Vautrot, M.; Ksiksi, N. Constitutive modelling effect on the numerical prediction of springback due to a stretch-bending test applied on titanium T40 alloy. *Arch. Civ. Mech. Eng.* **2015**, *15*, 836–846. [CrossRef]
15. Uemori, T.; Naka, T.; Tada, N.; Yoshimura, H.; Katahira, T.; Yoshida, F. Theoretical predictions of fracture and springback for high tensile strength steel sheets under stretch bending. *Procedia Eng.* **2017**, *207*, 1594–1598. [CrossRef]
16. Gu, Z.; Lv, M.; Li, X.; Xu, H. Stretch bending defects control of L-section aluminum components with variable curvatures. *Int. J. Adv. Manuf. Technol.* **2015**, *85*, 1053–1061. [CrossRef]
17. Han, S. Influence of Frictional Behavior Depending on Contact Pressure on Springback at U Draw Bending. *Trans. Mater. Process.* **2011**, *20*, 344–349. [CrossRef]
18. Fox, R.T.; Maniatty, A.M.; Lee, D. Determination of friction coefficient for sheet materials under stretch-forming conditions. *Met. Mater. Trans. A* **1989**, *20*, 2179–2182. [CrossRef]
19. Liu, K.X.; Liu, Y.L.; Yang, H. An analytical model for the collapsing deformation of thin-walled rectangular tube in rotary draw bending. *Int. J. Adv. Manuf. Technol.* **2013**, *69*, 627–636. [CrossRef]
20. Liu, K.; Liu, Y.; Yang, H. Experimental and FE simulation study on cross-section distortion of rectangular tube under multi-die constraints in rotary draw bending process. *Int. J. Precis. Eng. Manuf.* **2014**, *15*, 633–641. [CrossRef]
21. Liu, K.; Liu, Y.; Yang, H. Experimental study on the effect of dies on wall thickness distribution in NC bending of thin-walled rectangular 3A21 aluminum alloy tube. *Int. J. Adv. Manuf. Technol.* **2013**, *68*, 1867–1874. [CrossRef]
22. Guan, Y.; Zhao, J.; Wang, F.; Ma, L. Influence of friction on springback of plate tension-bending. *J. Plast. Eng.* **2003**, *10*, 43–45. [CrossRef]
23. Yang, H.; Li, H.; Zhan, M. Friction role in bending behaviors of thin-walled tube in rotary-draw-bending under small bending radii. *J. Mater. Process. Technol.* **2010**, *210*, 2273–2284. [CrossRef]
24. Zhang, Z.; Yang, Y.; Li, L.; Yin, J. Distribution of residual stress in an asymmetric T-section beam by stretch-bending. *Int. J. Mech. Sci.* **2019**, *164*, 105184. [CrossRef]
25. Muranaka, T.; Fujita, Y.; Otsu, M.; Haraguchi, O. Development of rubber-assisted stretch bending method for improving shape accuracy. *Procedia Manuf.* **2018**, *15*, 709–715. [CrossRef]
26. Liang, J.; Han, C.; Li, Y.; Yu, K.; Liang, C. Study on deformation difference between the contact zone and the non-contact zone of the flexible 3D stretch bending profile and roller dies based on pre-stretching amount. *Int. J. Adv. Manuf. Technol.* **2020**, *108*, 3579–3589. [CrossRef]
27. Hambleton, J.; Drescher, A. On modeling a rolling wheel in the presence of plastic deformation as a three- or two-dimensional process. *Int. J. Mech. Sci.* **2009**, *51*, 846–855. [CrossRef]
28. Bobrovskij, I.; Khaimovich, A.; Bobrovskij, N.; Travieso-Rodriguez, J.A.; Grechnikov, F. Derivation of the Coefficients in the Coulomb Constant Shear Friction Law from Experimental Data on the Extrusion of a Material into V-Shaped Channels with Different Convergence Angles: New Method and Algorithm. *Metals* **2022**, *12*, 239. [CrossRef]

29. Song, P.; Li, W.; Wang, X. A Study on Dynamic Plastic Deformation Behavior of 5052 Aluminum Alloy. *Key Eng. Mater.* **2019**, *812*, 45–52. [CrossRef]
30. *TS EN ISO 6892-1-2019*; Metallic Materials. Tensile Testing. Part 1: Method of Test at Room Temperature (ISO 6892-1-2019). ISO: Geneva, Switzerland, 2019. Available online: https://www.iso.org/standard/78322.html (accessed on 29 June 2022).
31. Bachchhav, B.; Bagchi, H. Effect of surface roughness on friction and lubrication regimes. *Mater. Today Proc.* **2020**, *38*, 169–173. [CrossRef]
32. Zhang, S.; Lv, G.; Ma, F.; Wang, Z.; Liu, Y. Influence of low-frequency vibration on friction coefficient of contact interface in bend-stretch forming. *Int. J. Light. Mater. Manuf.* **2022**, *5*, 306–314. [CrossRef]